Using mercury stable isotopes to quantify directional soil–atmosphere Hg(0) exchanges in rice paddy ecosystems: Implications for Hg(0) emissions to the atmosphere from land surfaces

Kun Zhang [a,b], Qiang Pu [a], Jiang Liu [c,a], Zhengdong Hao [a,b], Lijuan Zhang [d], Leiming Zhang [e], Xuewu Fu [a], Bo Meng [a,*], Xinbin Feng [a,b]

[a] *State Key Laboratory of Environmental Geochemistry, Institute of Geochemistry, Chinese Academy of Sciences, Guiyang 550081, China.*

[b] *University of Chinese Academy of Sciences, Beijing 100049, China.*

[c] *College of Resources, Sichuan Agricultural University, Chengdu 611130, China.*

[d] *Key Laboratory for Heavy Metal Pollution Control and Reutilization, School of Environment and Energy, Peking University Shenzhen Graduate School, Shenzhen, 518055, China.*

[e] *Air Quality Research Division, Science and Technology Branch, Environment and Climate Change Canada, Toronto, Ontario M3H 5T4, Canada.*

* Corresponding Author:

Bo Meng (mengbo@vip.skleg.cn)

Tel: +86-851-84396920, Fax: +86-851-85891721

ABSTRACT

Gaseous elemental mercury (Hg(0)) emissions from soils constitute a large fraction of global total Hg(0) emissions. However, existing studies do not distinguish biotic- and abiotic-mediated emissions and focus only on photoreduction mediated emissions, resulting in an underestimation of soil Hg(0) emissions into the atmosphere. In this study, directional mercury (Hg) reduction pathways in paddy soils were identified using Hg isotopes. Results showed significantly different isotopic compositions of Hg(0) between those yielded from photoreduction (δ^{202}Hg = −0.80 ± 0.34‰, Δ^{199}Hg = −0.38 ± 0.09‰), microbial reduction (δ^{202}Hg = −1.55 ± 0.10‰, Δ^{199}Hg = 0.29 ± 0.19‰), and abiotic dark reduction (δ^{202}Hg = −2.50 ± 0.12‰, Δ^{199}Hg = 0.50 ± 0.11‰). Hg(0) exchange fluxes between the atmosphere and the paddy soils were dominated by emissions, with the average flux ranging from 2.2 ± 5.7 to 16.8 ± 21.7 ng m^{-2} h^{-1} during different sampling periods. Using isotopic signatures based ternary mixed model, we revealed that photoreduction dominated Hg(0) emissions from paddy soils. Albeit lower, microbial and abiotic dark reductions contributed up to 34 ± 20% and 29 ± 17%, respectively, to Hg(0) emissions in certain periods. These novel findings can help improve future estimation of soil Hg(0) emissions from rice paddy ecosystems, which involve complex biotic-, abiotic-, and photo-reduction processes.

KEYWORDS: mercury reduction; mercury stable isotope; rice paddy; mercury emission

SYNOPSIS: This study identifies the relative contributions of directional Hg reduction pathways to Hg(0) emissions from paddy soils, providing future research directions for improving inventories of Hg(0) emissions from natural sources.

1. INTRODUCTION

Mercury (Hg) is a pollutant of global concern due to its persistence, neurotoxicity, and bioaccumulation.[1] Gaseous elemental mercury (Hg(0)) is the most abundant form of Hg in the atmosphere, and can be transported regionally and globally due to its extended atmospheric residence time (> 0.5 years).[2, 3] Atmospheric Hg(0) is released via both anthropogenic (e.g., mining and fossil fuel combustion) and natural processes (e.g., hydrothermal and volcanic activities, biomass burning, and re-emissions from legacy Hg on land and ocean surfaces).[4] Recent estimates of Hg emissions from anthropogenic sources are reasonably accurate, whereas those from natural sources still have large uncertainties[5, 6] due to a limited understanding of the air-surface Hg(0) exchange processes over different land uses.[4]

Given that terrestrial soils are the largest reservoir for natural and legacy anthropogenic Hg, accurately estimating global soil emissions is critical for assessing global Hg cycling.[7, 8] The 2018 Global Mercury Assessment showed that Hg(0) emissions from soil and vegetation accounted for 48% of natural Hg emissions from terrestrial ecosystems.[1] Photoreduction, microbial reduction, and abiotic dark reduction are considered the primary processes contributing to Hg(0) emissions from soils.[9] Solar radiation was considered the dominant factor for Hg reduction;[10-12] therefore, soil Hg(0) emissions are primarily assessed based on photoreduction process in chemical transport models.[2, 13, 14] Considering that microbial and abiotic dark reductions occur widely,[15] neglecting these processes may underestimate soil Hg(0) emissions. For example, ~ 60% of soil Hg(0) emissions was caused by microbial reductions in a subtropical forest,[9] and most soil Hg(0) emissions were caused by microbial and abiotic dark reductions in a remote subalpine forest.[16]

Wetlands play an important role in global Hg cycling and have become a net source of atmospheric Hg(0) due to declining atmospheric Hg concentrations.[17] Rice paddies are the largest human-made wetlands and account for approximately 18% of the global total wetlands.[18] Hg(II) reduction through photoreduction, microbial reduction, and abiotic dark reduction processes can lower the concentration of

substrates available for Hg methylation, and is thus a critical step of Hg cycling in paddy soils.[19-21] However, the relative importance of the above-mentioned reduction processes for Hg(0) emissions from paddy soils remains elusive, mainly due to traditional observations of Hg(0) concentration and exchange flux not being able to distinguish Hg(0) emitted from different reduction processes.

Mercury isotope geochemistry is a useful tool for tracing and quantifying the sources and biogeochemical pathways of Hg in natural environments.[22-24] A prerequisite of this approach is to obtain Hg isotopic compositions from different sources. Degrees of mass-dependent fractionations (MDF, expressed as δ^{202}Hg) and mass-independent fractionations (MIF, expressed as Δ^{199}Hg) were determined for various biotic and abiotic processes.[22] Previously, isotopic fractionation signatures of Hg(II) reduction processes were generated based on indoor experiments, instead of field conditions.[25-29] For microbial Hg(II) reduction processes, while the experiments showed an MDF, the degree of Hg isotope fractionation varied greatly (e.g., the enrichment factor ε^{202}Hg ranged from −1.20 to −2.00), as a result of differences in microbial Hg(0) reduction capacity and experimental conditions.[26, 27] Similarly, due to inconsistent experimental conditions, large ranges of MDF and MIF were observed in photoreduction experiments with ε^{202}Hg ranging from −0.60 to −1.72 and E^{199}Hg ranging from −0.43 to −3.73.[25, 28, 30-32] In contrast, relatively consistent Hg isotope fractionation was obtained for abiotic dark reduction processes with ε^{202}Hg ranging from −1.52 to −1.77 and E^{199}Hg ranging from 0.17 to 0.26.[28] Large uncertainties still exist in evaluating the contributions of various reduction processes to Hg(0) emissions from rice paddies using the Hg(0) isotopic compositions generated from the above-mentioned Hg(II) reduction experiments.

To address the issues summarized above, we conducted field studies followed by laboratory analysis to (1) determine Hg isotope fractionation of microbial reductions, photoreductions, and abiotic dark reductions, (2) characterize exchange fluxes and isotopic compositions of Hg(0) in the atmosphere–paddy soil exchange process using a dynamic flux chamber (DFC), and (3) quantify the relative contributions of different Hg(II) reduction processes to Hg(0) emissions from paddy soils. Results from this

study broaden the current understanding of the complex soil–atmosphere Hg(0) exchange processes in croplands and provide high-quality data supporting future estimates of natural Hg(0) emissions.

2. MATERIALS AND METHODS

2.1 Study Area and Sampling Site. Field experiments were performed in a paddy field (Gouxi, 109° 11′ 27″ E, 27° 33′ 48″ N) located in the Wanshan Hg mining area, in Guizhou Province, southwestern China. Gouxi was once one of the largest artisanal Hg mining centers in China.[33] Although large-scale Hg mining activities in the Wanshan Hg mining area ceased in 2003, Hg concentrations in the air (37.3–416 ng m^{-3},[34]) were consistently higher than the background value in Guizhou (2.8–8.2 ng m^{-3},[34]). Previous studies reported that in addition to significant methylation processes, Hg(II) reduction process was also active in paddy soils in this study area,[19-21] which may be the main cause for the consistently high atmospheric Hg(0) concentrations. Therefore, this artisanal Hg mining site was selected for examining soil–atmosphere Hg(0) flux exchanges.

2.2 Design of the indoor and field experiments. This study conducted indoor and field experiments to obtain Hg isotopic fractionation characteristics of different reduction processes, the isotopic compositions of the product Hg(0), and Hg(0) exchange fluxes between the atmosphere and paddy soils. All the experimental designs are described in detail below.

2.2.1 Isotopic Fractionation during the Microbial Reduction of Hg(II). The bacterial strain selected for this study was *Geobacter sulfurreducens* (*G. sulfurreducens*) PCA, which is a ubiquitous iron-reducing bacterium found in various ecosystems, including rice paddies.[35, 36] We have previously detected a high abundance of *G. sulfurreducens* PCA (accounting for 0.3% of the total bacteria population), which is the dominant Hg-reducing microorganism in the investigated paddy soils.[37] Therefore, it is reasonable to use *G. sulfurreducens* PCA to study isotope fractionation during the process of microbial reduction of Hg(II). The quality control details of the microbial reduction experiment are described in Text S1.

In the conditional experiments, dissolved organic matter (DOM) present in the overlying water of the rice paddy field cannot be removed by filtering through a 0.22 μm filter (Longjin, China). DOM was reported to be capable of reducing Hg(II) in the dark.[29] Therefore, deionized water (Milli-Q, Millipore, USA) was used in this experiment. In pure culture experiments, growth conditions of the PCA strain have been previously described.[38] Briefly, the strains were inoculated at 2% (*v/v*) in 200 mL of medium and cultured in an anaerobic bottle at 33°C in the dark (Figure S1). The PCA cells were collected at the exponential growth phase (~ 110 h), placed in a 2 mL sterilized centrifuge tube, centrifuged at 1500 × g for 10 min, and subsequently resuspended in phosphate buffer (PBS). The cells were separated equally into 33 anaerobic culture tubes (reactors) after washing three times in PBS and left to stand for 2 h before use in the Hg(II) reduction experiment. PBS was used as the reaction substrate. To obtain enough Hg for concentration and isotope analyses, 33 reactors with 10 mL of PBS were spiked with a NIST-3133 Hg(II) standard to reach an initial Hg(II) concentration of 20 ppb, according to the Hg tolerance curves of *G. sulfurreducens* PCA (Figure S2), and were placed in an oscillation incubator (THZ-98C, Yiheng, China) at a constant temperature of 33°C.

Anaerobic tubes were sampled for Hg isotope analyses at 0, 12, 16, 20, 24, 28, 32, 36, 40, 44, and 48 h after the experiment was initiated, using the sampling method shown in Figure S1 and described in a previous study.[39] Specifically, three anaerobic culture tubes were removed as parallel samples at each sampling time. The Hg(0) product in anaerobic culture tubes was preconcentrated into 5 mL of reverse aqua regia (40%, *v/v*, HNO_3:HCl = 3:1) by Hg-free N_2 at a flow rate of 100 mL min^{-1}. After purging, excess BrCl was added to the remaining solution to reach a concentration of 2.5% (*v/v*) to oxidize the remaining Hg in the anaerobic culture tubes to Hg(II). After > 24 h of oxidation, $NH_2OH{\cdot}HCl$ (25%, *w/v*) was added to the anaerobic culture tubes to reduce excess BrCl, followed by the addition of 1 mL of $SnCl_2$ solution to reduce the remaining Hg(II) to Hg(0). Similarly, reactant Hg(0) was obtained via preconcentration into 5 mL of 40% reverse aqua regia by Hg-free nitrogen at a flow

rate of 100 mL min^{-1} for 2 h. The Hg(0) samples were sealed and stored at 4°C in the dark for total Hg concentration and isotope analyses.

2.2.2 Isotopic Fractionation during Photoreduction and Abiotic Dark Reduction of Hg(II). As shown in Figure S3, *in-situ* photoreduction and abiotic dark reduction of Hg(II) were performed in the field from 10^{th} to 13^{th} of July, 2023. To eliminate the effects of microorganisms, cells in the overlying water of the rice paddy were removed using a 0.22 μm filter.[38, 40, 41] The sterile overlying water was divided into two precleaned PE boxes (30 L) with the water above the edge of the DFC to isolate ambient air. An air scrubber (Zero canister, Tekran) at the inlet of DFC was used as a source of Hg-free air.[42] Hg(0) samples were collected from the DFC outlet using a chlorine-impregnated activated carbon (CLC, mass: 0.6 g) trap with a flow rate of 1.0 − 2.0 L min^{-1}.[43] Two sets of experiments were conducted simultaneously with two DFC systems. During daytime, DFCs were exposed to natural sunlight to collect Hg(0) samples yielded from the photoreduction process, while at nighttime, DFCs were covered by light-tight boxes to collect Hg(0) samples yielded from the abiotic dark reduction process. During the experiment, 5 L of sterile overlying water was replaced every 6 h in the PE box to simulate the dynamic balance of Hg in the overlying water. Each Hg(0) sample collected from the DFC outlet represents a 12-h mixed sample under net emission conditions. Over a sampling period of 4 days, eight Hg(0) samples yielded from photoreduction during the daytime and another eight Hg(0) samples yielded from abiotic dark reduction during the nighttime were obtained. After completing the sampling, the CLC traps were plugged with Teflon stoppers and sealed with three clean polyethylene bags, stored in the dark, and shipped to the laboratory.

In the laboratory, the Hg(0) samples were preconcentrated from the CLC traps into 5 mL of 40% reverse aqua regia solution using the thermally desorbed method.[44] The trapping solutions were saved in a brown glass bottle and stored at 4°C in the dark before Hg concentration and isotopic composition analyses.

2.2.3 Hg0 Flux and Isotopic Compositions from Paddy Soil–Atmosphere Exchange. In 2021, Hg(0) exchange flux between the paddy soil and the atmosphere

was measured at Gouxi using the DFC method (Figure S4).[34, 45] Sampling was performed on the 50th , 90th, and 110th day after transplanting and first flooding, with each sampling period lasting 24 h. Soil moisture (water content on a dry mass basis) at a depth of 1 cm was 92 ± 8% on the 50th day and 102 ± 16% on the 90th day, and soil was drained and rice was harvested on the 110th day. Hg(0) samples from the DFC inlet and outlet were collected simultaneously using CLC traps with a flow rate of 1.0−2.0 L min^{-1}. The CLC traps in the DFC inlet and outlet were replaced every 6 h, i.e., each CLC trap represented a 6-h mixed sample. Twelve Hg(0) samples were collected from the DFC inlet and outlet, respectively. Similarly, the CLC traps were plugged with Teflon stoppers and sealed with three clean polyethylene bags, stored in the dark, and shipped to the laboratory for Hg concentration and isotopic composition analyses. Detailed sample information is shown in Table S3.

2.3 Chemical Analysis of Hg(0) and Hg(II) Concentrations and Isotopic Compositions. All CLC traps were preconcentrated into 5 mL of oxidizing solution of 40% reverse aqua regia using a tube muffle furnace.[42] Hg concentrations in the product and reactant trapping solutions were determined by $SnCl_2$ reduction and cold vapor atomic fluorescence spectrophotometry (CVAFS, Brooks Rand) according to US EPA 1631.[46]

The concentrations of Hg in the trapping solutions were diluted to 0.5-1 ng mL^{-1} for isotope analysis using a Nu-Plasma II multicollector inductively coupled plasma–mass spectrometer (MC-ICP-MS).[47] The NIST-3133 Hg standard solution was prepared at 0.5−1 ng mL^{-1} Hg in 10% HCl (v/v) and measured as a bracketing Hg standard in the same manner as the test samples. NIST-8610 secondary standard solutions were analyzed once after every 10 samples. The MDF of the Hg isotope is expressed using the δ^{xxx}Hg notation with reference to NIST-3133 (analyzed before and after every two samples) in accordance with Equation (1):

$$\delta^{xxx}\mathrm{Hg}(‰)=\left[\left(^{xxx}\mathrm{Hg}/^{198}\mathrm{Hg}\right)_{sample}/\left(^{xxx}\mathrm{Hg}/^{198}\mathrm{Hg}\right)_{NIST\text{-}3133}-1\right]\times 1000 \quad (1)$$

where *xxx* represents the mass number of Hg isotopes (199, 200, 201, and 202).[25] The MIF is expressed using the capital delta notation (Δ^{xxx}Hg) and calculated as Equation (2):[25]

$$\Delta^{xxx}\text{Hg}(‰)=\delta^{xxx}\text{Hg}-(\beta_{xxx}\times\delta^{202}\text{Hg}) \quad (2)$$

where the corresponding scaling factors β_{xxx} are 0.2520, 0.5024, and 0.7520 for ^{199}Hg, ^{200}Hg, and ^{201}Hg, respectively.

2.4. Data analysis

2.4.1 Mercury Mass Balance, Isotopic Balance, and Isotope Fractionation Characteristics in Microbial Reductions. The Hg mass and isotopic balance were measured during the microbial reduction experiment to assess the quality of the data. Given that the experimental system was closed and the process was irreversible, the sum of the Hg content and the Hg isotopes in the products and reactants during these processes should be consistent with the initial addition of Hg(II). Detailed calculation methods are provided in Text S2.

In the microbial reduction experiment, both the product Hg(0) and reactant Hg(II) followed MDF and Rayleigh fractionation modes. The kinetic fractionation factor (α^{202}) and the enrichment factor (ε^{202}) were determined from the experimental results using the Rayleigh distillation equation.[48] Detailed mathematical derivations are provided in Text S2.

2.4.2 Calculation of the Hg(0) Exchange Flux between the Atmosphere and Paddy Soils. Hg(0) exchange fluxes (F, ng m^{-2} h^{-1}) between the atmosphere and paddy fields were calculated using the following equation:

$$F=\frac{Q}{A}\times(C_o-C_i) \quad (3)$$

where C_o and C_i represent the Hg(0) concentrations (ng·m^{-3}) in the DFC outlet and inlet air, respectively, Q is the flow rate through the DFC (m^3·h^{-1}), and A is the area enclosed by the DFC (0.09 m^2).

2.4.3 Hg(0) Isotopic Compositions during the Paddy Soil–Atmosphere Exchange. MDF ($\delta^{202}\text{Hg}_{ex}$) and MIF ($\Delta^{199}\text{Hg}_{ex}$, $\Delta^{201}\text{Hg}_{ex}$) signatures for paddy soil–atmosphere Hg(0) exchanges were calculated following the method described by Zhu

et al.[34] Given the potential simultaneous occurrence of emission and deposition of Hg(0) in DFC, a modification factor (CMF) (ratio of $(C_o - C_i)/C_o$) was used to separate cases with significant Hg(0) emission (CMF > 0.15) and deposition (CMF < −0.15). The detailed information on the calculation method can be found in Text S3.

2.4.4 Source Apportionment Analysis. Based on the isotopic compositions of the product Hg(0) of the three main reduction processes (photoreduction, microbial reduction, and dark abiotic reduction) in paddy soils, a triple mixing model was constructed to evaluate the relative contributions of the three processes to Hg(0) emissions from paddy fields using Equations (4) – (6):

$$\delta^{202}Hg_s = \delta^{202}Hg_p \times F_p + \delta^{202}Hg_d \times F_d + \delta^{202}Hg_m \times F_m \quad (4)$$

$$\Delta^{199}Hg_s = \Delta^{199}Hg_p \times F_p + \Delta^{199}Hg_d \times F_d + \Delta^{199}Hg_m \times F_m \quad (5)$$

$$F_p + F_d + F_m = 1 \quad (6)$$

where δ^{202}Hg and Δ^{199}Hg with the subscripts *s*, *p*, *d*, and *m* represent the isotopic composition of Hg(0) emitted from paddy soils, Hg(0) yielded from photoreduction, dark abiotic reduction, and microbial reduction, respectively. F_p, F_d, and F_m are the contribution rates of Hg(0) yielded from the three reduction processes.

Given the uncertainty caused by the model parameters, a Monte Carlo simulation was performed to more accurately quantify the contribution rates of the three processes. A sample size of 100,000 isotopic compositions of Hg(0) yielded from different processes was selected randomly for model simulation using Equations (4)−(6). The simulation was completed using the MATLAB program, and the source code is shown in Text S4.

2.5 Quality Control and Statistical Analysis. During the analysis of Hg concentrations, the standard reference material (GBW07405) was treated in the same manner as for the CLC samples using the thermally desorbed method, with a Hg recovery of 100 ± 14% (1SD, n = 7). During the analysis of Hg isotopic compositions, the overall average and uncertainty of Hg isotopic compositions of NIST-8610 (δ^{202}Hg = –0.53 ± 0.03‰, Δ^{199}Hg = 0.00 ± 0.03‰, Δ^{200}Hg = 0.00 ± 0.04‰, Δ^{201}Hg = –0.03 ± 0.03‰, 1SD, n = 14) were found to agree with previous studies.[25, 49] During

the experiment on the microbial reduction of Hg(II), the sum of the product Hg(0) and the reactant Hg(II) remaining in the buffer, as calculated using Equation (S1) (Text S2), showed an 87.3 ~ 103.5% mass balance (Figure S5). The total Hg isotopic compositions calculated using Equations (S2) and (S3) in Text S2 (δ^{202}Hg = −0.03 ± 0.05‰ and Δ^{199}Hg = −0.01 ± 0.03‰, 1SD, n = 27) were highly consistent with the isotopic compositions of the initially added Hg(II) standard (NIST-3133) (Figure S6).

The data was plotted using Origin Pro 2018. Group differences were assessed using *t*-tests and one-way ANOVAs with Duncan's post hoc tests using SPSS Statistics 24 for Windows. Statistical significance (p) was set at < 0.05 (two-tailed).

3. RESULTS AND DISCUSSION

3.1 Mercury Isotope Fractionation Characteristics during the Microbial Reduction of Hg(II). With progression of the experiment of Hg (II) reduction by microbial bacteria, the proportion of Hg(II) in the reactant gradually decreased, while that of Hg(0) in the product gradually increased (Table S1). The product Hg(0), expressed as the percentage of the initially added Hg(II), reached a maximum value of ~ 80% 44 h after initiation of the experiment (Figure S5). Throughout the experiment, a good balance of Hg mass and isotope were obtained, indicating the reliability of the experimental design and results (Figures S5 and S6). For Hg isotope fractionation, a significant MDF (δ^{202}Hg from –1.60‰ to 1.50‰) and a nonsignificant MIF (Δ^{199}Hg from –0.17‰ to 0.18‰) were observed during microbial reduction of Hg(II) (Table S1, Figure S6). The product Hg(0) represented a lower δ^{xxx}Hg (*xxx* = 199, 200, 201, 202) than the reactant Hg(II) (Figure 1a), indicating that *G. sulfurreducens* PCA preferentially reduced the lighter isotopes of Hg as the reaction progressed. Both the product Hg(0) and the reactant Hg(II) followed a Rayleigh fractionation with experimental progression (Figure 1b). Detailed calculation methods for the fractionation factor for ^{202}Hg (α^{202}) and the enrichment factor associated with MDF (ε^{202}) are described in Text S2. During the microbial reduction of Hg(II) experiment, the α^{202} was 0.9993 ± 0.0001 (1SD), and ε^{202} was –0.70 ± 0.06‰ (1SD), the latter was lower than previously reported (ε^{202} range from –1.20 ± 0.10‰ to –2.00 ± 0.20‰,

288 2SD, [26, 27]), most likely due to differences in bacterial species and substrate Hg(II)
289 concentrations.[26, 27]

290 **3.2 Mercury Isotope Fractionation during Photoreduction and Abiotic Dark**
291 **Reduction Processes in Rice Paddies.** The isotopic signatures of the product Hg(0)
292 during the *in-situ* Hg(II) photoreduction and abiotic dark reduction processes are
293 shown in Table S2. The Hg(0) collected from the DFC outlet during daytime had a
294 δ^{202}Hg of –0.80 ± 0.34‰ and Δ^{199}Hg of –0.38 ± 0.09‰ (1SD, n = 8). Additionally,
295 the isotopic signatures of the outlet Hg(0) showed a Δ^{199}Hg/Δ^{201}Hg ratio of 1.07 (R^2 =
296 0.80, $p < 0.01$, Figure S7), implying that the emitted Hg(0) exhibited a signature
297 typical of photoreduction.[25] The Hg(0) from the DFC outlet during nighttime had a
298 δ^{202}Hg of –0.79 ± 0.29‰ and Δ^{199}Hg of –0.32 ± 0.16‰ (1SD, n = 8), which are
299 inconsistent with those reported in previous studies, especially for MIF.[28, 29] Abiotic
300 dark reduction of Hg(II) generally produces a small positive odd-MIF shift in the
301 product Hg(0).[28, 29] However, in the present study the average isotopic compositions
302 of the Hg(0) collected from the DFC outlet during nighttime were similar to those
303 collected during daytime, as can be seem from the signature values presented above.
304 This unexpected phenomenon was most likely caused by sunlight reaching to the
305 earth's surface, providing energy for the photoreduction of Hg(II) to Hg(0), which
306 was released slowly at nighttime.[45, 50]

307 **3.3 Atmosphere–Paddy Soil Hg(0) Exchange Fluxes.** The average (±1SD)
308 Hg(0) fluxes between the paddy soils and the atmosphere on the 50th, 90th, and 110th
309 day were 5.6 ± 10.8 ng m^{-2} h^{-1} (range: −7.8 to 18.4 ng m^{-2} h^{-1}), 16.8 ± 21.7 ng m^{-2}
310 h^{-1} (−9.0 to 38.8 ng m^{-2} h^{-1}), and 2.2 ± 5.7 ng m^{-2} h^{-1} (−5.1 to 7.7 ng m^{-2} h^{-1}),
311 respectively (Figure 2). Hg(0) emissions dominated the Hg(0) exchange fluxes
312 between the atmosphere and the paddy soils, especially during daytime. The soils
313 were not a significant sources of Hg(0), and were even a sink (flux < 0) of
314 atmospheric Hg(0) during nighttime. This phenomenon has also been observed in
315 many other vegetated canopies,[51] highlighting the role of solar radiation on Hg(0)
316 emissions.

It is noted that soil Hg(0) emission fluxes were significantly higher on the 90th than the 50th and 110th day ($p < 0.01$) (Figure 2). The stronger solar radiation on the 90th than 50th day likely played an important role in the higher Hg(0) emission on the 90th day through sunlight-induced processes (photoreduction and volatilization) that reduced Hg(II) to Hg(0) in rice paddy soils.[52, 53] The change in paddy soils from flooding to drying on the 110th day was possibly the main reason for the decreased Hg(0) emissions, since exchange fluxes between the soil and atmosphere can be minimized by low soil porosity in dry paddy soils.[21, 54] In addition, low penetration of solar radiation and a relatively aerobic environment could limit photoreduction and relevant biotic activities in dry paddy soils, resulting in low diffusion of Hg(0) to the atmosphere.[21, 54]

3.4 Estimation of the Contributions of Different Hg(II) Reduction Processes to Hg(0) Emissions from Rice Paddy Soils. Given that this study focused mainly on the emission of Hg(0) from paddy soils, only the samples with a CMF > 0.15 for the released Hg(0) isotopes are discussed here (Table S3). During the period of investigation, the mean isotopic compositions of Hg(0) collected from the DFC outlet (δ^{202}Hg = –0.48 ± 0.30‰, Δ^{199}Hg = –0.03 ± 0.07‰, 1SD, n = 7) were more negative than those of Hg(0) from the DFC inlet (δ^{202}Hg = 0.00 ± 0.33‰, Δ^{199}Hg = 0.04 ± 0.04‰, 1SD, n = 7), which may be caused by the emissions of Hg(0) from the paddy soil to the air.[42] Under net emission conditions, the mean Hg(0) isotopic compositions from the paddy soil–atmosphere exchange, as calculated using Equations (S6) and (S7) (Text S3), were as follows: $\delta^{202}Hg_{ex}$ = −1.22 ± 0.23‰ and $\Delta^{199}Hg_{ex}$ = −0.08 ± 0.10‰ (1SD, n = 3) on the 50th day, $^{202}Hg_{ex}$ = −0.81 ± 0.32‰ and $\Delta^{199}Hg_{ex}$ = −0.45 ± 0.04‰ (1SD, n = 2) on the 90th day, and $^{202}Hg_{ex}$ = −1.54 ± 0.53‰ and $\Delta^{199}Hg_{ex}$ = 0.06 ± 0.05‰ (1SD, n = 2) on the 110th day. These different Hg(0) isotopic compositions (especially odd–MIF) imply differences in reduction processes in paddy soils during the three sampling periods. This is because only photochemical processes can produce significant odd–MIF and abiotic dark reduction only produces small positive odd–MIF, whereas microbial reduction does not produce odd-MIF.[25-29]

The average Hg isotopic compositions of the overlying water (δ^{202}Hg = −0.85 ± 0.17‰, Δ^{199}Hg = 0.29 ± 0.19‰) in the investigated paddy field during the same sampling periods were reported by Yin et al.[55] The enrichment factor for microbial reduction (ε^{202}Hg = −0.7 ± 0.06‰, E^{199}Hg = 0) was determined in Section 3.1, and the enrichment factor for abiotic dark reduction experiments (ε^{202}Hg = −1.77‰ ~ −1.52‰, E^{199}Hg = 0.17‰ ~ 0.26‰) was obtained from Zheng and Hintelmann.[29] The isotopic compositions of Hg(0) yielded from microbial reduction (δ^{202}Hg = −1.55 ± 0.10‰, Δ^{199}Hg = 0.29 ± 0.19‰, 1SD) and abiotic dark reduction (δ^{202}Hg = −2.50 ± 0.12‰, Δ^{199}Hg = 0.50 ± 0.11‰, 1SD, Monte Carlo simulation) in the rice paddy were calculated using Equations (S8) and (S9) in Text S3 (Figure 3).

Based on a ternary mixed model, the relative contributions of different Hg(II) reduction processes associated with Hg(0) emissions from the rice paddy soil were evaluated using a Monte Carlo approach (Figure 4). Results showed that Hg(II) photoreduction, microbial reduction, and abiotic dark reduction contributed 55 ± 10%, 29 ± 16%, and 16 ± 10%, respectively, to the total Hg(0) emission from the rice paddy soil on the 50th day, and were 37 ± 9%, 34 ± 20%, and 29 ± 17%, respectively, on the 110th day. However, on the 90th day, the contribution of photoreduction was nearly 100% since the average isotopic compositions of the emitted Hg(0) were very close to the photoreduction endmember, meaning the contributions of the other two nonphotoreduction processes were almost negligible. This may not imply that photoreduction was the only process during this period, but rather that the effect of photoreduction was significantly stronger than that of the other two reduction processes. Moreover, the average Hg(0) emission fluxes were significantly higher during day- than nighttime on both the 50th and 90th day (as presented in Section 3.3), possibly because the rate of photoreduction was significantly higher than that of nonphotoreduction.[45] However, on the 110th day, the contribution of photoreduction decreased due to the low penetration of solar radiation in dry paddy soils,[54] while the relative contributions of microbial reduction and abiotic dark reduction increased correspondingly.

In current chemical transport models assessing terrestrial Hg(0) emissions, natural emissions rarely separate different Hg(II) reduction processes.[13, 56] Photoreduction is considered as the driving process of Hg(0) emissions from natural surfaces,[13, 14] which potentially bias the effects of different Hg(II) reduction processes on Hg(0) emissions.[57] Our results indicated that photoreduction was indeed the dominant factor affecting the Hg(0) emission from paddy soils on the 90th day; however, the contributions of microbial reduction and abiotic dark reduction during other periods cannot be ignored, and these processes should be considered in future assessment of Hg(0) emissions from farmland soils and even land surfaces. In addition, higher photoreduction contributions and higher Hg(0) emission fluxes occurred during the flood stage when compared to the drainage period, suggesting that broader wetland ecosystems may be important natural Hg(0) sources, whereas wetlands have long been recognized as Hg(0) sinks.[58]

4. ENVIRONMENTAL IMPLICATIONS

The ranges of isotopic fractionation caused by Hg(II) reduction processes, especially photoreduction, obtained from *in-situ* controlled experiments over a rice paddy soil were much smaller than previously reported values generated from laboratory-simulated experiments, probably due to different field and laboratory conditions. Although photoreduction is the dominant reduction pathway for Hg(0) emissions from paddy soils, microbial reduction and abiotic dark reduction pathways also contribute appreciable amounts of Hg(0) emissions under certain field conditions. Given that microbial reduction and abiotic dark reduction processes are widespread in natural environments, the contributions of these two reduction processes should be carefully considered when estimating inventories of Hg(0) emissions from natural sources to minimize uncertainties in Hg cycling assessments.

Although the rice paddy field used in this study is representative, the particularity of wet–dry alternation irrigation procedure of this type of field prevents the generalization of the results obtained from this study to other terrestrial landscapes. Therefore, future studies on the stable isotopic characteristics of Hg(0) emissions

from different types of terrestrial landscapes and large water bodies are needed to provide additional field data for constraining the estimates of natural Hg(0) emissions and calibrating global Hg cycling models. In particular, data from wetlands and lakes, which have received large amounts of historically exogenous Hg from atmospheric deposition or runoff,[58] are noteworthy.

ASSOCIATED CONTENT

Supporting Information

Additional experimental details are provided in Text S1-S4 and Table S1-S3. Additional figures as mentioned in the text in Figures S1-S7.

Notes

The authors declare no competing financial interest.

ACKNOWLEDGEMENTS

This research was supported by the National Natural Science Foundation of China (41931297). We thank Dr. Fang Fang from Peking University Shenzhen Graduate School for her help in the pure culture experiment. We also thank Dr. Hongqian Yin and M.S. Qianshuo Zhang for providing assistance in sample collection and determination. We thank Prof. Runsheng Yin and Prof. Mingmin Cui for their edits and comments on the draft of this manuscript.

REFERENCES

1. UNEP *Global Mercury Assessment 2018*; UN Environment Programme, Chemicals and Health Branch Geneva, Switzerland: 2019.
2. Horowitz, H. M.; Jacob, D. J.; Zhang, Y.; Dibble, T. S.; Slemr, F.; Amos, H. M.; Schmidt, J. A.; Corbitt, E. S.; Marais, E. A.; Sunderland, E. M., A new mechanism for atmospheric mercury redox chemistry: implications for the global mercury budget. *Atmos. Chem. Phys.* **2017,** *17*, (10), 6353-6371.
3. Schroeder, W. H.; Munthe, J., Atmospheric mercury - An overview. *Atmos Environ* **1998,** *32*, (5), 809-822.
4. Wang, X.; Lin, C. J.; Yuan, W.; Sommar, J.; Zhu, W.; Feng, X. B., Emission-dominated gas exchange of elemental mercury vapor over natural surfaces in China. *Atmospheric Chemistry and Physics* **2016,** *16*, (17), 11125-11143.
5. Pirrone, N.; Cinnirella, S.; Feng, X.; Finkelman, R. B.; Friedli, H. R.; Leaner, J.; Mason, R.; Mukherjee, A. B.; Stracher, G. B.; Streets, D. G.; Telmer, K., Global mercury emissions to the atmosphere from anthropogenic and natural sources. *Atmospheric Chemistry and Physics* **2010,** *10*, (13), 5951-5964.
6. Song, S.; Selin, N. E.; Soerensen, A. L.; Angot, H.; Artz, R.; Brooks, S.; Brunke, E. G.; Conley, G.; Dommergue, A.; Ebinghaus, R.; Holsen, T. M.; Jaffe, D. A.; Kang, S.; Kelley, P.; Luke, W. T.; Magand, O.; Marumoto, K.; Pfaffhuber, K. A.; Ren, X.; Sheu, G. R.; Slemr, F.; Warneke, T.; Weigelt, A.; Weiss-Penzias, P.; Wip, D. C.; Zhang, Q., Top-down constraints on atmospheric mercury emissions and implications for global biogeochemical cycling. *Atmospheric Chemistry and Physics* **2015,** *15*, (12), 7103-7125.
7. Obrist, D.; Kirk, J. L.; Zhang, L.; Sunderland, E. M.; Jiskra, M.; Selin, N. E., A review of global environmental mercury processes in response to human and natural perturbations: Changes of emissions, climate, and land use. *Ambio* **2018,** *47*, (2), 116-140.
8. Outridge, P. M.; Mason, R. P.; Wang, F.; Guerrero, S.; Heimbürger-Boavida, L. E.,

Updated Global and Oceanic Mercury Budgets for the United Nations Global Mercury Assessment 2018. *Environ Sci Technol* **2018,** *52*, (20), 11466-11477.

9. Yuan, W.; Wang, X.; Lin, C. J.; Wu, C. S.; Zhang, L. M.; Wang, B.; Sommar, J.; Lu, Z. Y.; Feng, X. B., Stable Mercury Isotope Transition during Postdepositional Decomposition of Biomass in a Forest Ecosystem over Five Centuries. *Environ Sci Technol* **2020,** *54*, (14), 8739-8749.
10. O'Connor, D.; Hou, D.; Ok, Y. S.; Mulder, J.; Duan, L.; Wu, Q.; Wang, S.; Tack, F. M. G.; Rinklebe, J., Mercury speciation, transformation, and transportation in soils, atmospheric flux, and implications for risk management: A critical review. *Environ Int* **2019,** *126*, 747-761.
11. Wang, S. F.; Feng, X. B.; Qiu, G. L.; Wei, Z. Q.; Xiao, T. F., Mercury emission to atmosphere from Lanmuchang Hg-Tl mining area, Southwestern Guizhou, China. *Atmos Environ* **2005,** *39*, (39), 7459-7473.
12. Zhu, J.; Wang, D.; Liu, X.; Zhang, Y., Mercury fluxes from air/surface interfaces in paddy field and dry land. *Appl Geochem* **2011,** *26*, (2), 249-255.
13. Smith-Downey, N. V.; Sunderland, E. M.; Jacob, D. J., Anthropogenic impacts on global storage and emissions of mercury from terrestrial soils: Insights from a new global model. *J Geophys Res-Biogeo* **2010,** *115*.
14. Zhang, Y. X.; Song, Z. C.; Huang, S. J.; Zhang, P.; Peng, Y. M.; Wu, P. P.; Gu, J.; Dutkiewicz, S.; Zhang, H. X.; Wu, S. L.; Wang, F. Y.; Chen, L.; Wang, S. X.; Li, P., Global health effects of future atmospheric mercury emissions. *Nat Commun* **2021,** *12*, (1).
15. Jiskra, M.; Wiederhold, J. G.; Skyllberg, U.; Kronberg, R. M.; Hajdas, I.; Kretzschmar, R., Mercury Deposition and Re-emission Pathways in Boreal Forest Soils Investigated with Hg Isotope Signatures. *Environ Sci Technol* **2015,** *49*, (12), 7188-7196.
16. Chen, C.; Huang, J.-H.; Li, K.; Osterwalder, S.; Yang, C.; Waldner, P.; Zhang, H.; Fu, X.; Feng, X., Isotopic Characterization of Mercury Atmosphere–Foliage and Atmosphere–Soil Exchange in a Swiss Subalpine Coniferous Forest. *Environ Sci Technol* **2023**.

17. Osterwalder, S.; Bishop, K.; Alewell, C.; Fritsche, J.; Laudon, H.; Åkerblom, S.; Nilsson, M. B., Mercury evasion from a boreal peatland shortens the timeline for recovery from legacy pollution. *Sci Rep-Uk* **2017,** *7*, (1), 16022.
18. Yoon, C. G., Wise use of paddy rice fields to partially compensate for the loss of natural wetlands. *Paddy Water Environ* **2009,** *7*, (4), 357-366.
19. Chen, J.; Hu, G. R.; Liu, J.; Poulain, A. J.; Pu, Q.; Huang, R.; Meng, B.; Feng, X. B., The divergent effects of nitrate and ammonium application on mercury methylation, demethylation, and reduction in flooded paddy slurries. *J Hazard Mater* **2023,** *460*.
20. Liu, J.; Chen, J.; Poulain, A. J.; Pu, Q.; Hao, Z. D.; Meng, B.; Feng, X. B., Mercury and Sulfur Redox Cycling Affect Methylmercury Levels in Rice Paddy Soils across a Contamination Gradient. *Environ Sci Technol* **2023,** *57*, (21), 8149-8160.
21. Wu, Q. Q.; Wang, B. L.; Hu, H. Y.; Bravo, A. G.; Bishop, K.; Bertilsson, S.; Meng, B.; Zhang, H.; Feng, X. B., Sulfate-reduction and methanogenesis are coupled to Hg(II) and MeHg reduction in rice paddies. *J Hazard Mater* **2023,** *460*.
22. Blum, J. D.; Sherman, L. S.; Johnson, M. W., Mercury Isotopes in Earth and Environmental Sciences. *Annual Review of Earth and Planetary Sciences* **2014,** *42*, (1), 249-269.
23. Kritee, K.; Motta, L. C.; Blum, J. D.; Tsui, M. T.-K.; Reinfelder, J. R., Photomicrobial Visible Light-Induced Magnetic Mass Independent Fractionation of Mercury in a Marine Microalga. *ACS Earth and Space Chemistry* **2017,** *2*, (5), 432-440.
24. Yin, R. S.; Feng, X. B.; Li, X. D.; Yu, B.; Du, B. Y., Trends and advances in mercury stable isotopes as a geochemical tracer. *Trends Environ Anal* **2014,** *2*, 1-10.
25. Bergquist, B. A.; Blum, J. D., Mass-dependent and -independent fractionation of Hg isotopes by photoreduction in aquatic systems. *Science* **2007,** *318*, (5849), 417-420.
26. Kritee, K.; Blum, J. D.; Barkay, T., Mercury stable isotope fractionation during

511 reduction of Hg(II) by different microbial pathways. *Environ Sci Technol* **2008,** *42*,
512 (24), 9171-9177.
513 27. Kritee, K.; Blum, J. D.; Johnson, M. W.; Bergquist, B. A.; Barkay, T., Mercury
514 Stable Isotope Fractionation during Reduction of Hg(II) to Hg(0) by Mercury
515 Resistant Microorganisms. *Environ Sci Technol* **2007,** *41*, (6), 1889-1895.
516 28. Zheng, W.; Hintelmann, H., Mercury isotope fractionation during photoreduction
517 in natural water is controlled by its Hg/DOC ratio. *Geochim Cosmochim Ac* **2009,**
518 *73*, (22), 6704-6715.
519 29. Zheng, W.; Hintelmann, H., Nuclear Field Shift Effect in Isotope Fractionation of
520 Mercury during Abiotic Reduction in the Absence of Light. *Journal of Physical*
521 *Chemistry A* **2010,** *114*, (12), 4238-4245.
522 30. Motta, L. C.; Chien, A. D.; Rask, A. E.; Zimmerman, P. M., Mercury Magnetic
523 Isotope Effect: A Plausible Photochemical Mechanism. *Journal of Physical*
524 *Chemistry A* **2020,** *124*, (19), 3711-3719.
525 31. Rose, C. H.; Ghosh, S.; Blum, J. D.; Bergquist, B. A., Effects of ultraviolet
526 radiation on mercury isotope fractionation during photo-reduction for inorganic
527 and organic mercury species. *Chemical Geology* **2015,** *405*, 102-111.
528 32. Zheng, W.; Hintelmann, H., Mass independent isotope fractionation of mercury
529 during its photochemical reduction by low-molecular-weight organic compounds.
530 *Geochim Cosmochim Ac* **2010,** *74*, (12), A1224-A1224.
531 33. Meng, B.; Feng, X.; Qiu, G.; Liang, P.; Li, P.; Chen, C.; Shang, L., The process of
532 methylmercury accumulation in rice (Oryza sativa L.). *Environ Sci Technol* **2011,**
533 *45*, (7), 2711-7.
534 34. Zhu, W.; Fu, X.; Zhang, H.; Liu, C.; Skyllberg, U.; Sommar, J.; Yu, B.; Feng, X.,
535 Mercury Isotope Fractionation during the Exchange of Hg(0) between the
536 Atmosphere and Land Surfaces: Implications for Hg(0) Exchange Processes and
537 Controls. *Environ Sci Technol* **2021,** *56*, (2), 1445-1457.
538 35. Ding, L. Y.; He, N. N.; Yang, S.; Zhang, L. J.; Liang, P.; Wu, S. C.; Wong, M. H.;
539 Tao, H. C., Inhibitory effects of Skeletonema costatum on mercury methylation by
540 Geobacter sulfurreducens PCA. *Chemosphere* **2019,** *216*, 179-185.

36. Liu, Y. R.; Johs, A.; Bi, L.; Lu, X.; Hu, H. W.; Sun, D.; He, J. Z.; Gu, B. H., Unraveling Microbial Communities Associated with Methylmercury Production in Paddy Soils. *Environ Sci Technol* **2018,** *52*, (22), 13110-13118.
37. Zhang, R.; Aris-Brosou, S.; Storck, V.; Liu, J.; Abdelhafiz, M. A.; Feng, X.; Meng, B.; Poulain, A. J., Mining-impacted rice paddies select for Archaeal methylators and reveal a putative (Archaeal) regulator of mercury methylation. *ISME Communications* **2023,** *3*, (1), 74.
38. Hu, H.; Lin, H.; Zheng, W.; Rao, B.; Feng, X.; Liang, L.; Elias, D. A.; Gu, B., Mercury Reduction and Cell-Surface Adsorption by Geobacter sulfurreducens PCA. *Environ Sci Technol* **2013,** *47*, (19), 10922-10930.
39. Zhang, W.; Sun, G. Y.; Yin, R. S.; Feng, X. B.; Yao, Z. X.; Fu, X. W.; Shang, L. H., Separation of methylmercury from biological samples for stable isotopic analysis. *Journal of Analytical Atomic Spectrometry* **2021,** *36*, (11), 2415-2422.
40. Gu, B. H.; Bian, Y. R.; Miller, C. L.; Dong, W. M.; Jiang, X.; Liang, L. Y., Mercury reduction and complexation by natural organic matter in anoxic environments. *P Natl Acad Sci USA* **2011,** *108*, (4), 1479-1483.
41. Richard, A.; Delvaux, J.; Bourel-Bonnet, L., Effects of sterilizing-grade filters on the physico-chemical properties of onion-like vesicles. *Int J Pharmaceut* **2006,** *312*, (1-2), 144-150.
42. Yuan, W.; Wang, X.; Lin, C. J.; Sommar, J. O.; Wang, B.; Lu, Z. Y.; Feng, X. B., Quantification of Atmospheric Mercury Deposition to and Legacy Re-emission from a Subtropical Forest Floor by Mercury Isotopes. *Environ Sci Technol* **2021,** *55*, (18), 12352-12361.
43. Fu, X.; Heimbürger, L. E.; Sonke, J. E., Collection of atmospheric gaseous mercury for stable isotope analysis using iodine- and chlorine-impregnated activated carbon traps. *Journal of Analytical Atomic Spectrometry* **2014,** *29*, 841-852.
44. Huang, Q.; Liu, Y. L.; Chen, J. B.; Feng, X. B.; Huang, W. L.; Yuan, S. L.; Cai, H. M.; Fu, X. W., An improved dual-stage protocol to pre-concentrate mercury from airborne particles for precise isotopic measurement. *Journal of Analytical Atomic*

Spectrometry **2015,** *30*, (4), 957-966.

45. Zhang, H.; Fu, X. W.; Wu, X.; Deng, Q. W.; Tang, K. H.; Zhang, L. M.; Sommar, J.; Sun, G. Y.; Feng, X. B., Using Mercury Stable Isotopes to Quantify Bidirectional Water-Atmosphere Hg(0) Exchange Fluxes and Explore Controlling Factors. *Environ Sci Technol* **2023,** *57*, (29), 10673-10685.
46. USEPA, Method 1631, Revision E: Mercury in Water by Oxidation, Purge and Trap, and Cold Vapor Atomic Fluorescence Spectrometry. **2002**.
47. Yin, R. S.; Feng, X. B.; Foucher, D.; Shi, W. F.; Zhao, Z. Q.; Wang, J., High Precision Determination of Mercury Isotope Ratios Using Online Mercury Vapor Generation System Coupled with Multi-collector Inductively Coupled Plasma-Mass Spectrometry. *Chinese J Anal Chem* **2010,** *38*, (7), 929-934.
48. Criss, R. E., *Principles of Stable Isotope Distribution*. Oxford University Press: 1999.
49. Sun, G. Y.; Sommar, J.; Feng, X. B.; Lin, C. J.; Ge, M. F.; Wang, W. G.; Yin, R. S.; Fu, X. W.; Shang, L. H., Mass-Dependent and -Independent Fractionation of Mercury Isotope during Gas-Phase Oxidation of Elemental Mercury Vapor by Atomic Cl and Br. *Environ Sci Technol* **2016,** *50*, (17), 9232-9241.
50. Gustin, M. S.; Ericksen, J. A.; Schorran, D. E.; Johnson, D. W.; Lindberg, S. E.; Coleman, J. S., Application of controlled mesocosms for understanding mercury air-soil-plant exchange. *Environ Sci Technol* **2004,** *38*, (22), 6044-6050.
51. Zhang, L.; Wright, L. P.; Blanchard, P., A review of current knowledge concerning dry deposition of atmospheric mercury. *Atmos Environ* **2009,** *43*, (37), 5853-5864.
52. Fu, X. W.; Feng, X. B.; Yin, R. S.; Zhang, H., Diurnal variations of total mercury, reactive mercury, and dissolved gaseous mercury concentrations and water/air mercury flux in warm and cold seasons from freshwaters of southwestern China. *Environmental Toxicology and Chemistry* **2013,** *32*, (10), 2256-2265.
53. Zhu, J. S.; Wang, D. Y.; Liu, X. A.; Zhang, Y. T., Mercury fluxes from air/surface interfaces in paddy field and dry land. *Appl Geochem* **2011,** *26*, (2), 249-255.
54. Fu, X. W.; Feng, X. B.; Zhang, H.; Yu, B.; Chen, L. G., Mercury emissions from natural surfaces highly impacted by human activities in Guangzhou province,

South China. *Atmos Environ* **2012,** *54*, 185-193.

55. Yin, H. Q.; Yao, H.; Yuan, W.; Lin, C. J.; Fu, X. W.; Yin, R. S.; Meng, B.; Luo, J.; Feng, X. B., Determination of the Isotopic Composition of Aqueous Mercury in a Paddy Ecosystem Using Diffusive Gradients in Thin Films. *Anal Chem* **2023,** *95*, (33), 12290-12297.

56. Zhang, Y. X.; Zhang, P.; Song, Z. C.; Huang, S. J.; Yuan, T. F.; Wu, P. P.; Shah, V. R.; Liu, M. D.; Chen, L.; Wang, X. J.; Zhou, J.; Agnan, Y., An updated global mercury budget from a coupled atmosphere-land-ocean model: 40% more re-emissions buffer the effect of primary emission reductions. *One Earth* **2023,** *6*, (3), 316-325.

57. Sun, R. Y.; Jiskra, M.; Amos, H. M.; Zhang, Y. X.; Sunderland, E. M.; Sonke, J. E., Modelling the mercury stable isotope distribution of Earth surface reservoirs: Implications for global Hg cycling. *Geochim Cosmochim Ac* **2019,** *246*, 156-173.

58. Zhang, J.; Li, C.; Tang, W.; Wu, M.; Chen, M.; He, H.; Lei, P.; Zhong, H., Mercury in wetlands over 60 years: Research progress and emerging trends. *Sci Total Environ* **2023,** *869*, 161862.

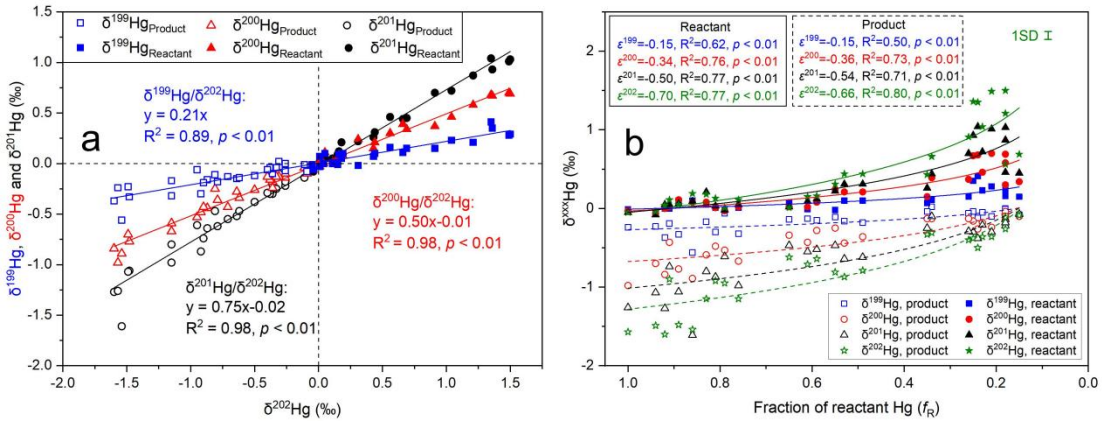

Figure 1. (a) Mass dependence on fractionation. δ^{199}Hg *vs* δ^{202}Hg, δ^{200}Hg *vs* δ^{202}Hg, and δ^{201}Hg *vs* δ^{202}Hg for the reactor and trap samples. (b) Rayleigh plots of δ^{xxx}Hg (*xxx* = 199, 200, 201, 202) as a function of f_R. The colored solid and dashed lines are modeled Rayleigh curves based on Equation (S4) in Text S2 for δ^{199}Hg, δ^{200}Hg, δ^{201}Hg, and δ^{202}Hg, respectively. The green error bar represents ± 1 standard deviation for the δ^{202}Hg of NIST-8610.

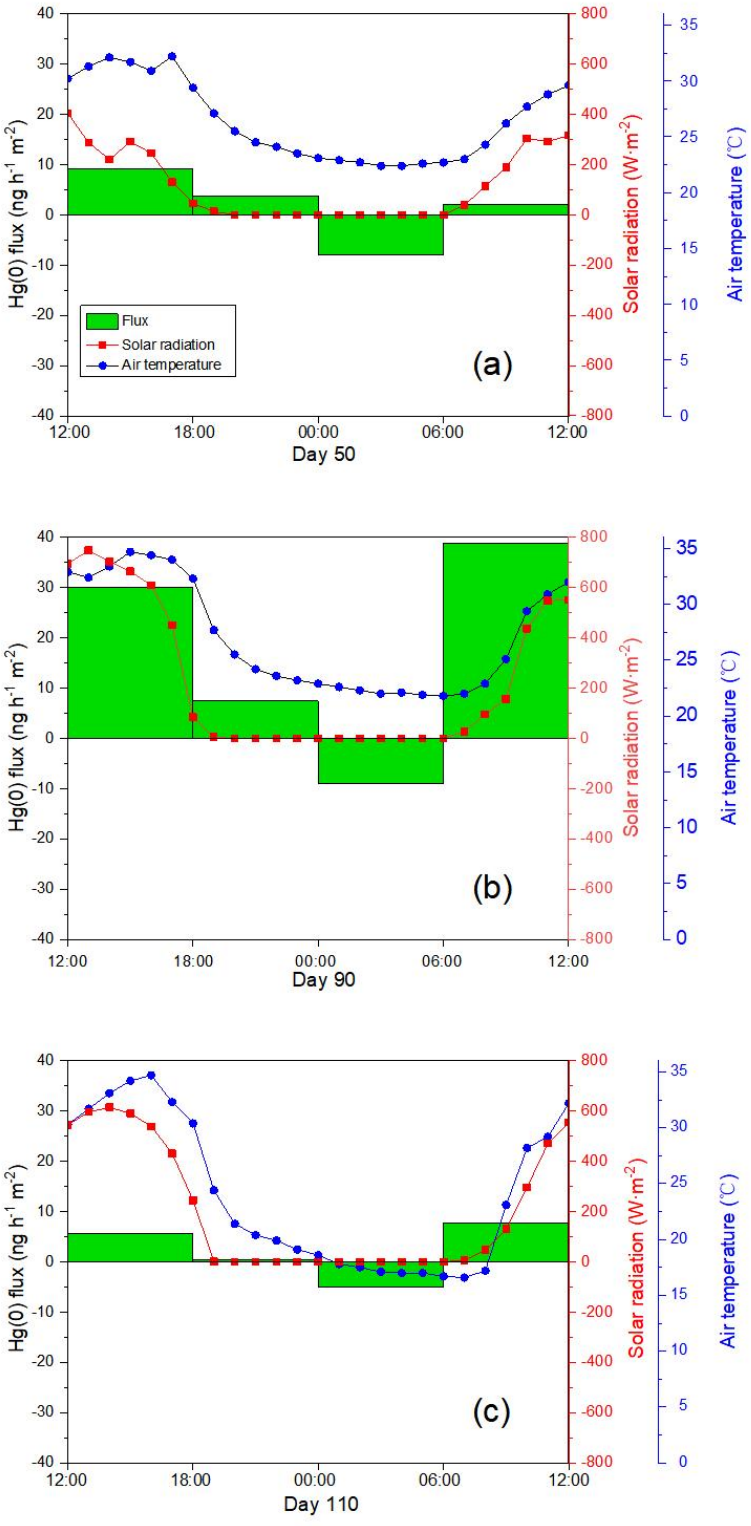

626

627 **Figure 2.** Diurnal variations of atmosphere–paddy soil Hg(0) exchange fluxes and
628 meteorological parameters.

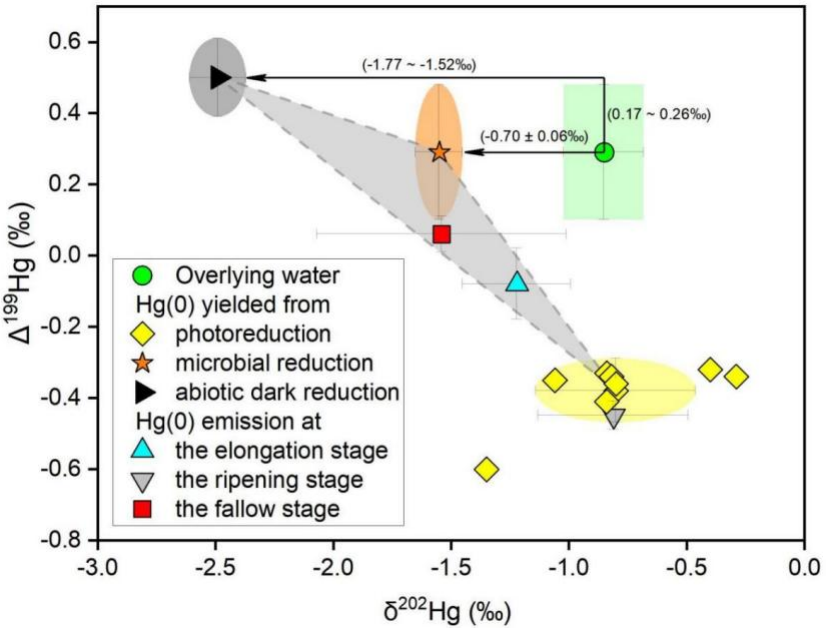

629

630 **Figure 3.** Hg isotopic compositions (Δ^{199}Hg versus δ^{202}Hg) of exchanged Hg(0)
631 between paddy soils and the atmosphere. Error bars indicate the 1SD analytical
632 uncertainty. Arrows represent the enrichment processes from the overlying water to
633 the endmembers (microbial reduction and abiotic dark reduction).

634

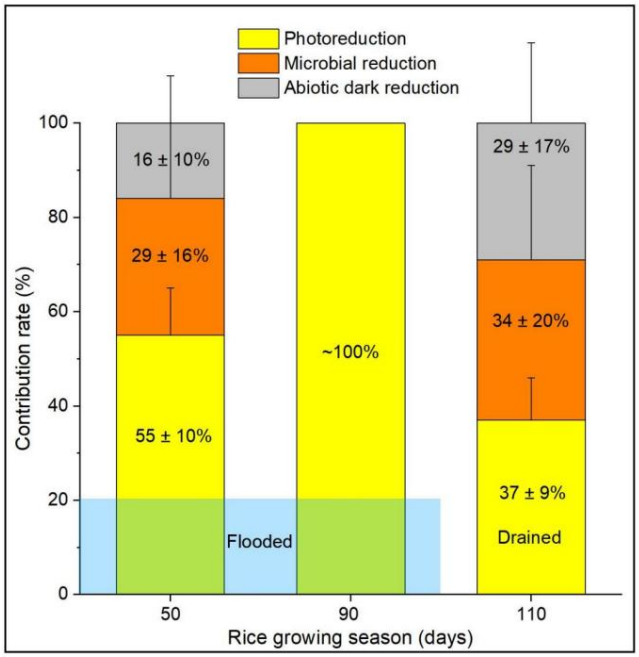

Figure 4. Contribution rates of three Hg(II) reduction processes to Hg(0) emissions from paddy soils at different sampling times.